Anisotropy and polarization of x-ray line emissions in the dielectronic recombination of hydrogenlike Fe^{25+} ions

Zhihao Yang,[1,2,*] Junwen Gao,[1,*] Wenmin Yan,[2,3] Ke Yao,[4] Jiamin Yang,[2] Zhongwen Wu,[5] and Zhimin Hu[1,†]

[1]*Key Laboratory of Radiation Physics and Technology of Ministry of Education, Institute of Nuclear Science and Technology, Sichuan University, Chengdu 610064, China*

[2]*Laser Fusion Research Center, China Academy of Engineering Physics, Mianyang 621900, China*

[3]*Institute of Atomic and Molecular Physics, Jilin University, Changchun 130012, China*

[4]*Shanghai EBIT Laboratory, Institute of Modern Physics, and Key Laboratory of Nuclear Physics and Ion-Beam Application (MOE), Fudan University, Shanghai 200433, China*

[5]*Key Laboratory of Atomic and Molecular Physics and Functional Materials of Gansu Province, College of Physics and Electronic Engineering, Northwest Normal University, Lanzhou 730070, China*

(Received 8 April 2021; accepted 30 July 2021; published 10 August 2021)

We present a systematic study of the anisotropy and polarization of x-ray line emissions in *KLL* dielectronic recombination of hydrogenlike Fe^{25+} ions. For the *KLL* dielectronic recombination considered, it consists of a resonant electron capture plus a two-step radiative decay. While the anisotropy and polarization of the first-step decay photons are calculated by using the flexible atomic code, those of the second-step decay photons are obtained with two methods, i.e., the formalism of the deorientation factor and density matrix theory. Resonance strengths are presented as well to synthesize the dielectronic satellite line spectra. The synthetic spectra including the correction of anisotropy and polarization effects show better agreement with existing experiments than previous calculations. This indicates that these effects are important for the intensity distribution of the dielectronic satellite lines.

DOI: 10.1103/PhysRevA.104.022809

I. INTRODUCTION

The $K\alpha$ lines of highly charged Fe ions are of great interest and importance in the fields of astrophysics and astronomy. Owing to their high relative abundance, high transition rate, and low intergalactic absorption, the Fe $K\alpha$ lines constitute the most prominent feature of astrophysical x-ray spectra. They are encoded with a variety of rich physical dynamics information and are often used to study x-ray binaries [1] and active galactic nuclei [2–4]. From their generation to being observed, they usually travel a long journey in the universe, i.e., passing by massive celestial objects and/or passing through interstellar dust, all of which will leave imprints on their feature. Therefore, the Fe $K\alpha$ lines are also often used to study gravitational lenses [5], interstellar polarization [6], and other effects [7,8].

The x-ray lines observed in the field of astrophysics may be polarized, especially when emitted from anisotropic plasmas. Anisotropic plasmas exist widely in solar flares [9], pulsars [10], and neutron stars [11], as well as around accreting black holes [12]. Polarization can provide insight into the geometric information on the direction in which x-ray lines are generated. Therefore, it can be used to reveal the orientation of electron or ion beams and magnetic field in plasmas. It is also closely related to some interesting astronomical phenomena [13,14]. Since its first observation streaming from the Crab Nebula [15], polarization of x rays has always attracted a great deal of attention from astronomers. For example, it can be used to determine the axis of a spinning pulsar [16]. Moreover, most of the mysterious fast radio bursts [17] are also strongly linearly polarized.

To explain polarized spectral lines, a profound understanding of the population mechanism of excited states is required. Usually, directional particle-beam collision excitation [18,19], dielectronic recombination (DR) [20], etc., may generate polarized lines.

Dielectronic recombination is one of the important electron-ion collision processes in hot plasmas. As a dominant recombination process, DR possesses large total cross sections which are several orders of magnitude larger than other recombination processes. Therefore, it can significantly affect the ionization balance and energy-level population of hot plasmas. Furthermore, the doubly excited states formed in the DR process are mainly stabilized by radiative decay rather than Auger decay, especially for highly charged heavy ions. As a consequence, the line emissions due to DR strongly affect the $K\alpha$ spectral lines in hot plasmas. In addition, due to a strong sensitivity of dielectronic satellite lines to temperature and density, they have been intensively used in diagnosing the properties of hot plasmas in astrophysics [21], tokamaks [22,23], and inertial confinement fusion [24].

Recently, anisotropy and polarization of dielectronic satellite lines have attracted attention due to the potential applications in both atomic collisions and plasma diagnosis.

*These authors contribute equally to this work.

†huzhimin@scu.edu.cn

For instance, anisotropy measurement of spectral lines has been used to study the details of electron-electron interactions in DR. A dominant contribution of the Breit interaction was theoretically predicted by Fritzsche *et al.* [25], which was soon demonstrated by Hu *et al.* [26,27]. To understand the underlying mechanism of the unexpected effect caused by the Breit interaction, polarization and anisotropy measurements of spectral lines following DR into highly charged ions were also made by Jörg *et al.* [28], Shah *et al* [29], and Amaro *et al.* [30]. Moreover, Tong *et al.* [31] and Li *et al.* [32] performed detailed theoretical analyses on this issue, and a comprehensive review was presented by Nakamura [33]. Besides the Breit interaction, Shah *et al.* [34] also investigated higher-order resonant contributions to x-ray line polarization and claimed that polarization measurement could be a useful approach to diagnose the electron temperature of hot plasmas. Furthermore, Shah *et al.* [35] stated that polarization of DR satellite lines could be used in diagnosing anisotropies of hot celestial plasmas.

Note that all the studies mentioned above are only for heliumlike and higher-Z-like ions. In addition, Zakowicz *et al.* [36] calculated the angular distribution and correlation of the two-step decay photons emitted in the KLL DR of hydrogenlike ions, in which only the electric dipole ($E1$) channel was taken into account. Later on, Fritzsche *et al.* and Matula *et al.* performed a series of calculations of this kind [37–39] within the framework of the density matrix theory [40]. These calculations show that a multipole mixing between the dominant $E1$ and higher-order radiative decay channels can significantly change the angular distribution and polarization properties for high-Z ions. Up to the present, however, there are no experimental measurements to confirm these theoretical calculations. Furthermore, DR resonance strengths of hydrogenlike ions have been measured for argon [41], titanium [42,43], krypton [44], and uranium [45]. Apart from the measurement for hydrogenlike uranium [45], the others need an anisotropy correction in simulating the corresponding DR resonance strengths because the x rays were observed at specific angles. A highly-spectra-resolved measurement of dielectronic satellite lines of hydrogenlike iron has been done by Nakamura *et al.* [46]. Nevertheless, the anisotropy and polarization effects could not be considered at that time and thus a large deviation between experiment and theory was shown.

In the present work we study the KLL DR spectra of hydrogenlike iron. We focus on the anisotropy and polarization of the DR spectral lines. To do so, DR resonance strengths are calculated using the flexible atomic code (FAC) [47]. The anisotropy and polarization are calculated taking into account both the multipole effect and the relativistic effect due to the Breit interaction in order to compare with the experimental line intensity measured by a polarization-sensitive crystal spectrometer at an electron beam ion trap. The present theoretical line intensity is given by multiplying the DR resonance strength, anisotropy, and correction factor of crystal diffraction. The synthetic spectrum is obtained by convolving the theoretical line intensity with the experimental resolution and the natural width of lines, which generally reproduces experimental spectrum within the experimental uncertainty.

II. THEORY

In general, DR is considered as a two-step resonant radiative recombination process, i.e., resonant dielectronic capture plus subsequent radiative stabilization. To be specific, a free electron with appropriate kinetic energy is captured by an ion A^{q+} with charge state q along with an excitation of an inner-shell electron, resulting in the ion being in a doubly excited state $A^{(q-1)+**}$. Subsequently, the ion in the doubly excited state decays into a singly excited state by first-step radiative transition and it decays further by second-step transition if there is still an inner-shell vacancy left. For the KLL DR of hydrogenlike ions considered herein, it can be expressed as

$$\begin{aligned} e + A^{q+}(1s) &\rightarrow A^{(q-1)+**}(2l2l') \\ &\rightarrow A^{(q-1)+*}(1s2l') + \hbar\nu \\ &\rightarrow A^{(q-1)+}(1s^2) + \hbar\nu + \hbar\nu'. \end{aligned} \tag{1}$$

Two photons with slightly different energies are emitted in this process, in which the first-step photon $\hbar\nu$ is emitted from the transition between the doubly excited state $|d\rangle$ and the singly excited state $|s\rangle$, and the second-step one ($\hbar\nu'$) is emitted in the decay from the singly excited state $|s\rangle$ to the ground state $|g\rangle$.

A. Resonance strength

The resonance strength of an isolated DR from an initial state $|i\rangle$ via a doubly excited state $|d\rangle$ to a singly excited state $|s\rangle$ can be expressed as

$$S_{ids} = \int_0^\infty \sigma_{ids}(E)dE = \frac{g_d}{2g_i}\frac{\pi^2\hbar^3 A^a_{di}}{m_e E_r}\frac{A^r_{ds}}{\sum A^r + \sum A^a}, \tag{2}$$

where E_r is the resonant energy, $\hbar$ is the reduced Plank constant, m_e is the electron mass, g_d and g_i are the statistical weights of the states $|d\rangle$ and $|i\rangle$, respectively, A^r_{ds} is the Einstein coefficient for spontaneous emission from the state $|d\rangle$ to the state $|s\rangle$, and A^a_{di} is the autoionization rate from the state $|d\rangle$ to $|i\rangle$. The summation runs over all the possible autoionization and radiative decay channels from the doubly excited state $|d\rangle$.

B. Alignment and its transfer in cascade decay

Alignment parameters are often used to describe the magnetic sublevel population of excited ions, which determine the polarization and angular distribution of the spectral lines emitted in the radiative decay of the ions. The alignment parameters are angle dependent, but only the values at the direction perpendicular to the electron beam ($\vartheta = 90^\circ$ and $\varphi = 0$) are discussed in this work. Specifically, the alignment parameters of the doubly excited state can be expressed in terms of the population density of the magnetic sublevels [48]

$$\begin{aligned} \mathcal{A}^d_k = \sum_{M_d} (-1)^{J_d+M_d}[(2k+1)(2J_d+1)]^{1/2} \\ \times \begin{pmatrix} J_d & J_d & k \\ -M_d & M_d & 0 \end{pmatrix} \sigma_{M_d}. \end{aligned} \tag{3}$$

Here k is the rank, J_d is the total angular momentum of the intermediate doubly excited state $|d\rangle$, σ_{M_d} is the population

density of the sublevel $|J_d M_d\rangle$ normalized with $\sum_{M_d} \sigma_{M_d} = 1$, M_d is the magnetic quantum number ranging from $-J_d$ to J_d with an interval 1, and $(\vdots\,\vdots\,\vdots)$ denotes the Wigner $3j$ symbol.

The singly excited state $|s\rangle$ would be still aligned if its angular momentum is greater than one after the first-step radiative decay. In this case, the alignment of the singly excited state $|s\rangle$ is determined by the first-step radiative decay from the doubly excited state $|d\rangle$, and the corresponding alignment transfer can be described by the deorientation factor [48]

$$U_k(J_d, J_s, L) = (-1)^{J_d+J_s+k+L}[(2J_d+1)(2J_s+1)]^{1/2} \times \begin{Bmatrix} J_d & J_d & k \\ J_s & J_s & L \end{Bmatrix}. \tag{4}$$

Here J_d and J_s are the total angular momenta of the doubly and singly excited states, respectively. $L = 1$ for $E1$ and magnetic dipole ($M1$) transitions, while $L = 2$ for magnetic quadrupole ($M2$) transitions. $\{\vdots\,\vdots\,\vdots\}$ denotes the Wigner $6j$ symbol. With the use of the deorientation factor (4), the alignment parameters of the singly excited state $|s\rangle$ can be written as

$$\mathcal{A}_k^s = \mathcal{A}_k^d U_k(J_d, J_s, L), \tag{5}$$

where $\mathcal{A}_k^d$ is the alignment parameters (3) of the doubly excited state $|d\rangle$.

Alternatively, within the framework of the density matrix theory, the alignment parameters of the singly excited state $|s\rangle$ following the first-step radiative decay can also be given by [39]

$$\mathcal{A}_{k_2 q_2}^s = W_{1\mathrm{st}}^{-1} \sum_{k_1 k} g_{k_1 k_2 k}^{ds} \mathcal{A}_k^d \times \langle k_1 - q_2 k_2 q_2 | k 0\rangle Y_{k_1,-q_2}\Big(\frac{\pi}{2}, 0\Big). \tag{6}$$

Here $W_{1\mathrm{st}}$ is the angular distribution coefficient of the first-step decay photons, $\langle k_1 - q_2 k_2 q_2 | k 0\rangle$ is the Clebsch-Gordan coefficient, $Y_{k_1,-q_2}(\frac{\pi}{2}, 0)$ are the spherical harmonics, and $g_{k_1 k_2 k}^{ds}$ is the so-called generalized structure function [39], which for a particular radiative transition $|d\rangle \to |s\rangle$ can be expressed as

$$g_{k_1 k_2 k}^{ds} = \frac{1}{4\sqrt{\pi}}[J_d, J_s]^{1/2}(-1)^{L+1}[1+(-1)^{k_1}][k_2, L, L]^{1/2} \times \langle L1L-1|k_1 0\rangle \begin{Bmatrix} J_d & J_d & k \\ J_s & J_s & k_2 \\ L & L & k_1 \end{Bmatrix}. \tag{7}$$

Here $[a, b, c, \ldots] \equiv (2a+1)(2b+1)(2c+1)\cdots$, $\{\vdots\,\vdots\,\vdots\}$ is the Wigner $9j$ symbol, k_2 $(=2, 4, \ldots)$ is the multipole order corresponding to the second-step decay photons, and the k_1 are even integers restricted by $|k - k_2| \leqslant k_1 \leqslant k + k_2$.

C. Anisotropy and polarization of x-ray line emissions

The anisotropy of emitted x-ray lines can be described by the corresponding angular distribution coefficient, which is generally expressed as

$$W = 1 + \sum_{k=2,4,\ldots} \sum_{q=-k}^{k} \sqrt{\frac{4\pi}{2k+1}} \beta_{kq} Y_{k,q}(\vartheta, \varphi), \tag{8}$$

with

$$\beta_{kq} = f_k \mathcal{A}_{kq}. \tag{9}$$

Here f_k is the structure function of the corresponding radiative transition and is given by [39]

$$f_k = \sqrt{4\pi}\sqrt{2k+1}\, g_{k0k}. \tag{10}$$

For the first-step radiative decay, due to an axial symmetry of the decay system, only $\mathcal{A}_{k0}^d$ with a zero component is nonvanishing. Therefore, the corresponding angular distribution coefficient at the direction perpendicular to the electron beam can be simplified to be

$$W_{1\mathrm{st}} = 1 - \tfrac{1}{2}\alpha_2^{ds}\mathcal{A}_2^d + \tfrac{3}{8}\alpha_4^{ds}\mathcal{A}_4^d. \tag{11}$$

Here α_k is the intrinsic anisotropy parameter [49,50]

$$\alpha_k(J_i, J_f, L) = (-1)^{J_i+J_f-1}\sqrt{(2k+1)(2J_i+1)}(2L+1) \times \begin{pmatrix} L & L & k \\ 1 & -1 & 0 \end{pmatrix} \begin{Bmatrix} L & L & k \\ J_i & J_i & J_f \end{Bmatrix}. \tag{12}$$

It should be noted that α_k is nonvanishing only when k is less than twofold the total angular momentum of the upper level of the transition, i.e., $k \leqslant 2J_i$.

For the second-step radiative decay, the calculation of the corresponding angular distribution coefficient is similar to that for the first-step one if the deorientation factor (4) is used and the parameters $\mathcal{A}_k^d$ and α_k^{ds} are replaced with $\mathcal{A}_k^s$ and α_k^{sg}, respectively. Moreover, the angular distribution coefficient corresponding to the second-step decay can be calculated also by using the density matrix theory, although such a calculation becomes relatively complex. For this case, all the alignment parameters $\mathcal{A}_{kq}^s$ with both zero and nonzero components are required as the decay system loses its axial symmetry due to the first-step radiative decay and therefore the corresponding angular distribution coefficient at the direction perpendicular to the electron beam reads

$$W_{2\mathrm{nd}} = W_{1\mathrm{st}}\Bigg\{1 + \alpha_2^{sg}\sqrt{\frac{4\pi}{5}}\sum_{q=-2}^{2}\mathcal{A}_{2q}^s Y_{2q}\Big(\frac{\pi}{2}, 0\Big) + \alpha_4^{sg}\sqrt{\frac{4\pi}{9}}\sum_{q=-4}^{4}\mathcal{A}_{4q}^s Y_{4q}\Big(\frac{\pi}{2}, 0\Big)\Bigg\}. \tag{13}$$

It should be noted that for transitions with $J_d < 2$ or via dipole channels, the third term in Eqs. (11) and (13) disappears.

Apart from the angular distribution coefficient, the degree of linear polarization of the first-step photons can be expressed as

$$P = \mp\frac{3\alpha_2^{ds}\mathcal{A}_2^d}{2 - \alpha_2^{ds}\mathcal{A}_2^d}, \tag{14}$$

where the minus (plus) sign corresponds to $E1$ ($M1$) transitions. Moreover, for quadrupole radiative transitions, the degree of linear polarization is given by

$$P = \pm\frac{12\alpha_2^{ds}\mathcal{A}_2^d + 5\alpha_4^{ds}\mathcal{A}_4^d}{8 - \left(4\alpha_2^{ds}\mathcal{A}_2^d - 3\alpha_4^{ds}\mathcal{A}_4^d\right)}. \tag{15}$$

Here the plus (minus) sign corresponds to $E2$ ($M2$) transitions.

For the second-step radiative decay, the calculation of the degree of linear polarization is similar to that for the first-step one if the deorientation factor is used, but it is relatively complex if using density matrix theory. Specifically, for dipole photons it can be expressed as [50]

$$P = \mp \frac{\sqrt{\frac{3}{2}}\alpha_2^{sg} \sum_q \mathcal{A}_{2q}^s \left[D_{q2}^{2*}\left(0, \frac{\pi}{2}, 0\right) + D_{q-2}^{2*}\left(0, \frac{\pi}{2}, 0\right)\right]}{1 + \alpha_2^{sg}\sqrt{\frac{4\pi}{5}} \sum_q \mathcal{A}_{2q}^s Y_{2q}\left(\frac{\pi}{2}, 0\right)}. \tag{16}$$

In this expression, D_{mn}^k denotes the Wigner D function and the minus (plus) sign corresponds to $E1$ ($M1$) transitions. For quadrupole decay photons, moreover, their degree of linear polarization is given by

$$P = \pm \left\{ \sqrt{\frac{3}{2}}\alpha_2^{sg} \sum_{q=-2}^{2} \mathcal{A}_{2q}^s \left[D_{q2}^{2*}\left(0, \frac{\pi}{2}, 0\right) + D_{q-2}^{2*}\left(0, \frac{\pi}{2}, 0\right)\right] - \sqrt{\frac{5}{8}}\alpha_4^{sg} \sum_{q=-4}^{4} \mathcal{A}_{4q}^s \left[D_{q2}^{4*}\left(0, \frac{\pi}{2}, 0\right) + D_{q-2}^{4*}\left(0, \frac{\pi}{2}, 0\right)\right] \right\} \times \frac{1}{W}. \tag{17}$$

Again, the plus (minus) sign corresponds to $E2$ ($M2$) transitions and W is given by Eq. (13).

III. CALCULATION

A. Configuration-interaction method and Breit interaction

The present calculation is implemented by using the FAC package based on the configuration-interaction method. In this method, an atomic-state function (ASF) with parity Π, total angular momentum J, magnetic quantum number M, and additional quantum numbers γ for a unique specification of the state is expressed as a linear combination of configuration-state functions (CSFs) with the same ΠJM as follows:

$$\Psi(\gamma \Pi JM) = \sum_{r=1}^{n} c_r \Phi(\gamma_r \Pi JM). \tag{18}$$

Here n is the number of CSFs used for constructing the ASF; c_r denotes the configuration mixing coefficients, which are obtained by diagonalizing the model Hamiltonian matrix. The CSFs are constructed as an antisymmetrized sum of the products of one-electron Dirac spinors. In the present calculation, all the configurations $nlnl$ with n and n' up to 7 are taken into account.

Moreover, the Hamiltonian of an atomic or ionic system with N electrons can be expressed in atomic units as

$$H = \sum_{i=1}^{N} H_D(i) + \sum_{i<j}^{N} V_{ij}^{ee}, \tag{19}$$

where $H_D(i)$ is the Dirac Hamiltonian of the ith electron and V_{ij}^{ee} is the interaction potential between the ith and jth electrons. Usually, the Coulomb interaction $V_{ij}^C = 1/r_{ij}$ between electrons dominates V_{ij}^{ee}. However, for highly charged ions the well-known Breit interaction could greatly modify the inter-electronic interaction, resulting in a drastic change of atomic structure and properties [51]. The Breit interaction consists of two parts, i.e., the magnetic interaction

$$V_{ij}^{\text{mag}} = -\boldsymbol{\alpha}_i \cdot \boldsymbol{\alpha}_j \frac{\cos(\omega_{ij} r_{ij})}{r_{ij}} \tag{20}$$

and the retardation interaction

$$V_{ij}^{\text{ret}} = (\boldsymbol{\alpha}_i \cdot \boldsymbol{\nabla}_i)(\boldsymbol{\alpha}_j \cdot \boldsymbol{\nabla}_j) \frac{\cos(\omega_{ij} r_{ij}) - 1}{\omega_{ij}^2 r_{ij}}, \tag{21}$$

where $\boldsymbol{\alpha}_i$ are the Dirac matrices, r_{ij} is the interelectronic distance, and ω_{ij} denotes the frequency of the exchanged virtual photon. By including the Breit interaction in the interelectronic interaction, the so-called Dirac-Coulomb-Breit Hamiltonian can be obtained as

$$H_{\text{DCB}} = \sum_{i=1}^{N} H_D(i) + \sum_{i<j}^{N} \left(V_{ij}^C + V_{ij}^{\text{mag}} + V_{ij}^{\text{ret}}\right), \tag{22}$$

which is used in the present calculations to include the contribution of the Breit interaction.

B. Relative intensity of x-ray line emission

For the first-step radiative decay, the intensity $I_{1\text{st}}$ of emission line is related to the resonance strength S_{idf} as

$$I_{1\text{st}} \propto S_{ids} \cdot W_{1\text{st}}, \tag{23}$$

where $W_{1\text{st}}$ is the angular distribution coefficient of the first-step photons at the direction perpendicular to the electron beam. However, for the second-step decay the intensity $I_{2\text{nd}}$ of the associated emission line is given by

$$I_{2\text{nd}} \propto S_{ids} \cdot B \cdot W_{2\text{nd}}, \tag{24}$$

where $W_{2\text{nd}}$ is the angular distribution coefficient of the second-step photons at the direction perpendicular to the electron beam, which is calculated by taking the cascade effect into account, and B is the branching ratio of the transition from the singly excited state $|s\rangle$ to the ground state $|g\rangle$ and can be expressed as

$$B = \frac{A_{sg}^r}{\sum A^r}. \tag{25}$$

Since the emitted x-ray lines may be anisotropic and polarized, the observed spectra should be adjusted by accounting for the efficiency dependence of the crystal spectrometer used on polarization. The intensity of x-ray spectral lines observed with the crystal spectrometer at 90° relative to the electron beam direction is given by [48]

$$I^{\text{obs}} = R_{\parallel} I_{\parallel} + R_{\perp} I_{\perp}. \tag{26}$$

Here $I_{\parallel}$ and $I_{\perp}$ are intensity components of the lines defined by the electric field vector parallel and perpendicular to the electron beam, respectively, and $R_{\parallel}$ and $R_{\perp}$ are the integrated reflectivity of crystal for x rays polarized parallel and perpendicular to the plane of dispersion (note that this plane is perpendicular to the electron beam), respectively. By means of the intensity components $I_{\parallel}$ and $I_{\perp}$, the degree of linear polarization of the x-ray lines emitted at 90° relative to the

electron beam can be also defined as

$$P = \frac{I_\parallel - I_\perp}{I_\parallel + I_\perp}, \tag{27}$$

while the total intensity of the emission lines is given by

$$I = I_\parallel + I_\perp. \tag{28}$$

Therefore, the observed intensity of x-ray lines with the crystal spectrometer can be obtained as

$$I^{\rm obs} = \frac{I}{2}[1 + P + R(1 - P)]R_\parallel, \tag{29}$$

where $R = R_\perp/R_\parallel$ and it depends on the Bragg angle θ_B (or, equivalently, on the photon energy E). For the energy range that we are interested in, the following linear dependence of R on the Bragg angle θ_B is considered:

$$R = 1.393\,96 - 0.030\,85 \cdot \theta_B. \tag{30}$$

This dependence is obtained by linearly fitting the calculated values with x-ray oriented program software [52] at some data points, which is in good agreement with that from Beiersdorfer *et al.* [48].

C. Synthesis of spectra

For comparing with experimental spectra, the theoretical intensities of x-ray lines obtained herein are convolved with the experimental resolution. Moreover, since the higher-multipole decay channels in radiative transitions can interfere with the $E1$ one and thus may cause a strong anisotropy for some x-ray lines in high-Z ions but less pronounced in medium-Z ions [39], only the contributions of higher multipole are incorporated in obtaining synthetic spectra. After considering the discussion above, the synthetic spectra can be given by

$$\mathcal{L}(E) = \sum_{\text{all lines}} I^{\rm obs} \cdot V(E), \tag{31}$$

where the summation runs over all the lines involved and $V(E)$ is the Voigt profile function

$$V(E) = \frac{2\ln 2}{\pi\sqrt{\pi}} \frac{\Gamma}{w^2} \int_{-\infty}^{\infty} \frac{e^{-t^2}}{(x - t)^2 + a^2} dt. \tag{32}$$

In this function, $a = \frac{\sqrt{\ln 2}\Gamma}{w}$, $x = \frac{2\sqrt{\ln 2}(E - E_0)}{w}$, and Γ is the natural width of transition lines,

$$\Gamma = \hbar(A_1 + A_2). \tag{33}$$

Moreover, w is the energy resolution of the crystal spectrometer and is given as

$$w = \frac{\Delta\theta_B}{\tan(\theta_B)} E \approx \frac{\Delta x \cdot E}{D \tan(\theta_B)}, \tag{34}$$

where Δx is the source size and D is the work distance of the crystal spectrometer.

IV. RESULTS AND DISCUSSION

The capture of a free electron in initially hydrogenlike Fe^{25+} ions is the first step of the DR process, which brings the ions into heliumlike Fe^{24+} ions in doubly excited states. The

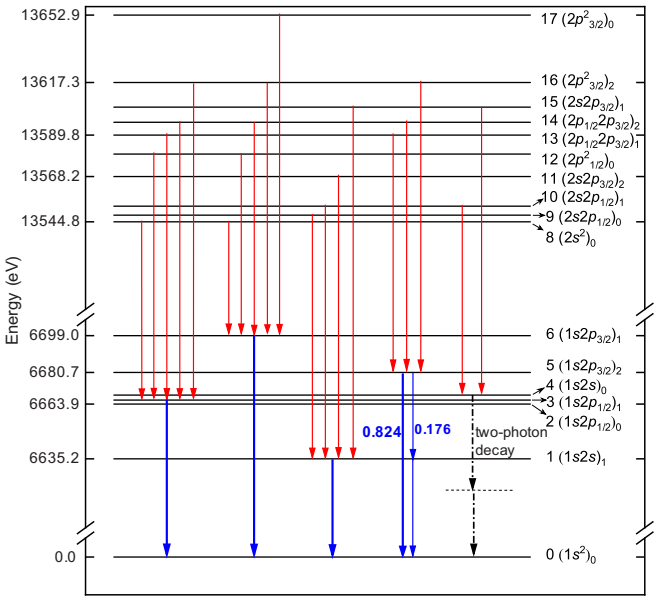

FIG. 1. Diagram of energy levels and dominant radiative transitions. The solid red arrows represent the transitions from doubly excited states to singly excited states and the solid blue arrows indicate those from singly excited states to ground states directly or via some intermediate states. The dash-dotted black arrows label a two-photon decay.

Fe^{24+} ions in doubly excited states decay radiatively to the ground state via various singly excited states, leading to the emission of two-step $K\alpha$ photons. The dominant transitions involved in the two-step radiative decay are diagramed in Fig. 1. The red arrows indicate the first-step radiative decays from doubly excited states to singly excited states, while the blue arrows represent the second-step ones from the singly excited states to the ground state directly or via some intermediate states. Moreover, the dash-dotted arrows indicate two-photon decays, which will be discussed in Sec. IV B.

The DR resonance strengths of hydrogenlike Fe^{25+} ions are obtained using the atomic data generated by the FAC package. In the calculations, each of the DR processes for individual channels is dealt with separately and the contributions from higher multipoles are included. By considering the anisotropy and polarization as well as the correction of polarization-sensitive diffraction efficiency of the crystal spectrometer, the synthetic spectra are obtained for comparison with the experimental spectra [46]. In the experiment, hydrogenlike Fe^{25+} ions were produced by keeping the electron beam energy at a 14 keV cooking energy for 300 ms. The electron beam energy was then quickly switched to 5.5 keV and scanned with a triangular waveform between 5.5 and 4.3 keV, which covers the KLL DR resonances of hydrogenlike Fe^{25+}. The duration of the electron energy scan was 0.5 ms and then the electron beam energy was quickly switched back to the 14 keV cooking energy and kept there for 7 ms. Every 1.5 s, all the trapped ions were dumped to prevent accumulation of unwanted ions.

TABLE I. Calculated resonance strengths S_{1st}, resonance energies E_{res}, photon energies $\hbar\nu$, branching ratios B from the doubly excited state $|d\rangle$ to the singly excited state $|s\rangle$, angular distribution coefficients W at 90° relative to the electron beam, and correction factors K_c for the crystal diffraction efficiency of the first-step photons. The doubly and singly excited states are indexed by the numbers before them. Here S_{1st} is in units of 10^{-20} cm^2 eV and all the energies are in eV.

$\|d\rangle$		$\|s\rangle$		Transition	E_{res}	$\hbar\nu$	B	W	S_{1st}	K_c
8	$(2s^2)_0$	6	$(1s2p_{3/2})_1$	$K\alpha_1^h$	4718.1	6845.8	0.131	1	1.174	0.798
12	$(2p_{1/2}^2)_0$			$K\alpha_1^h$	4753.2	6881.0	0.019	1	0.003	0.795
14	$(2p_{1/2}2p_{3/2})_2$			$K\alpha_2^h$	4769.7	6897.4	0.146	1.130	2.411	0.868
16	$(2p_{3/2}^2)_2$			$K\alpha_1^h$	4790.6	6918.3	0.531	1.162	18.175	0.881
17	$(2p_{3/2}^2)_0$			$K\alpha_1^h$	4826.2	6953.9	0.943	1	0.688	0.790
13	$(2p_{1/2}2p_{3/2})_1$	5	$(1s2p_{3/2})_2$	$K\alpha_2^h$	4763.1	6909.2	0.415	0.998	0.010	0.792
14	$(2p_{1/2}2p_{3/2})_2$			$K\alpha_2^h$	4769.7	6915.8	0.422	0.870	5.356	0.698
16	$(2p_{3/2}^2)_2$			$K\alpha_1^h$	4790.6	6936.7	0.172	0.838	4.246	0.670
10	$(2s2p_{1/2})_1$	4	$(1s2s)_0$	$K\alpha_2^h$	4725.8	6886.2	0.033	0.936	0.069	0.750
15	$(2s2p_{3/2})_1$			$K\alpha_1^h$	4777.6	6937.9	0.576	1.498	12.276	1.000
8	$(2s^2)_0$	3	$(1s2p_{1/2})_1$	$K\alpha_2^h$	4718.1	6878.9	0.116	1	1.045	0.795
12	$(2p_{1/2}^2)_0$			$K\alpha_2^h$	4753.2	6914.1	0.970	1	0.141	0.793
13	$(2p_{1/2}2p_{3/2})_1$			$K\alpha_1^h$	4763.1	6923.9	0.229	1.009	0.006	0.798
14	$(2p_{1/2}2p_{3/2})_2$			$K\alpha_1^h$	4769.7	6930.5	0.260	1.130	4.291	0.864
16	$(2p_{3/2}^2)_2$			$K\alpha_1^h$	4790.6	6951.4	0.001	1.162	0.026	0.877
9	$(2s2p_{1/2})_0$	1	$(1s2s)_1$	$K\alpha_2^h$	4721.0	6912.6	0.905	1	0.679	0.793
10	$(2s2p_{1/2})_1$			$K\alpha_2^h$	4725.8	6917.4	0.873	1.032	1.987	0.812
11	$(2s2p_{3/2})_2$			$K\alpha_1^h$	4741.5	6933.1	0.944	1.174	2.349	0.885
15	$(2s2p_{3/2})_1$			$K\alpha_1^h$	4777.6	6969.2	0.023	0.751	0.242	0.584

A. First-step radiative decays

The resonance strengths corresponding to the first-step radiative decays are listed in Table I together with other atomic parameters. As can be seen from the table, the resonant dielectronic capture of hydrogenlike Fe^{25+} ions gives rise to ten doubly excited states of the resulting heliumlike Fe^{24+} ions, which decay radiatively to five singly excited states by emitting the first-step photons. Now we arrive at the obtained branching ratios (BRs) of these doubly excited states to the singly excited ones. It is found that except for the doubly excited state $(2s^2)_0$ that has a relatively small total radiative BR of 0.247 [consisting of 0.116 to $(1s2p_{1/2})_1$ and 0.131 to $(1s2p_{3/2})_1$], the respective total BRs of other doubly excited states are all larger than 0.5. For example, the total BRs of the states $(2p_{3/2}^2)_0$ and $(2p_{1/2}^2)_0$ are nearly 1. This indicates that the great majority of the doubly excited states decay radiatively instead of nonradiatively. It should be noted that all radiative transitions from those doubly excited states with total angular momentum $J_d = 0$ have an angular distribution coefficient of 1 as the states with $J_d = 0$ possess only one magnetic sublevel. Moreover, both the radiative transitions $(2p_{3/2}^2)_2 \rightarrow (1s2p_{3/2})_1$ and $(2s2p_{3/2})_1 \rightarrow (1s2s)_0$ are found to have the strongest resonance strengths and thus will contribute dominantly to the x-ray spectra.

Figure 2 shows the first-step synthetic spectra obtained herein together with the contributions from individual transition components. As seen clearly from the figure, there are seven peaks in the synthetic spectra. Except for the two peaks centered at 1.787 and 1.792 Å, almost every other peak corresponds to a single transition. It is found that the peak at 1.787 Å consists of four transitions $(2p_{1/2}2p_{3/2})_2 \rightarrow (1s2p_{1/2})_1$, $(2s2p_{3/2})_2 \rightarrow (1s2s)_1$, $(2p_{3/2}^2)_2 \rightarrow (1s2p_{3/2})_2$, and $(2s2p_{3/2})_1 \rightarrow (1s2s)_0$, while the one at 1.792 Å mainly consists of five other transitions $(2p_{3/2}^2)_2 \rightarrow (1s2p_{3/2})_1$, $(2s2p_{1/2})_0 \rightarrow (1s2s)_1$, $(2s2p_{1/2})_1 \rightarrow (1s2s)_1$, $(2p_{1/2}2p_{3/2})_2 \rightarrow (1s2p_{3/2})_2$, and $(2p_{1/2}^2)_0 \rightarrow (1s2p_{1/2})_1$ and the contribution of other transitions to this peak is almost negligible. For the two peaks, the energies of their respective transition components are too close to be resolved. Nevertheless, the contributions from each individual transition component to these two peaks are listed in Table II for further reference.

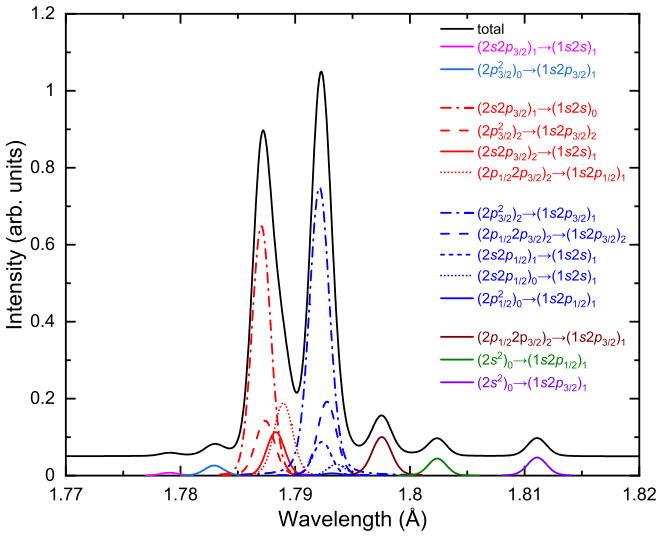

FIG. 2. The DR spectra obtained corresponding to the first-step decay photons. The colored lines show the spectra associated with individual transitions, while the black line indicates the overall spectra. For a clear display, the black line is shifted up by 0.05.

TABLE II. Contribution of each individual transition to the two main peaks centered at 1.787 and 1.792 Å

$\|d\rangle$		$\|s\rangle$		S_{1st}	Contribution
Peak at 1.787 Å (6938.11 eV)					
14	$(2p_{1/2}2p_{3/2})_2$	3	$(1s2p_{1/2})_1$	4.291	18.53%
11	$(2s2p_{3/2})_2$	1	$(1s2s)_1$	2.349	10.14%
16	$(2p^2_{3/2})_2$	5	$(1s2p_{3/2})_2$	4.246	18.33%
15	$(2s2p_{3/2})_1$	4	$(1s2s)_0$	12.276	53.00%
Peak at 1.792 Å (6918.75 eV)					
16	$(2p^2_{3/2})_2$	6	$(1s2p_{3/2})_1$	18.175	68.96%
9	$(2s2p_{1/2})_0$	1	$(1s2s)_1$	0.679	2.57%
10	$(2s2p_{1/2})_1$	1	$(1s2s)_1$	1.987	7.54%
14	$(2p_{1/2}2p_{3/2})_2$	5	$(1s2p_{3/2})_2$	5.356	20.33%
12	$(2p^2_{1/2})_0$	3	$(1s2p_{1/2})_1$	0.141	0.53%
others				0.016	0.07%

B. Second-step radiative decays

Due to the fact that there is still a vacancy left in the K shell after the first-step radiative decay, a second photon will be emitted in the second-step radiative decay from the singly excited states to the ground state. As discussed above, ten doubly excited states decay to five singly excited states, while only four singly excited states decay to the ground state with the emissions of the second-step x-ray photons. A special case is that the singly excited state $(1s2s)_0$ is strictly forbidden due to the angular momentum and parity selection rules, although it can decay to the ground state by simultaneously emitting two $E1$ photons [53,54],

$$(1s2s)_0 \rightarrow (1s^2)_0 + \hbar\nu_1 + \hbar\nu_2. \tag{35}$$

The two photons share the transition energy between the states $(1s2s)_0$ and $(1s^2)_0$, which have no contribution to the second-step synthetic spectra. Another special case in the second-step radiative decay is that the state $(1s2p_{3/2})_2$ can decay directly to the ground state or via the intermediate state $(1s2s)_1$ with a BR of 0.176 to the ground state $(1s^2)_0$, as shown in Fig. 1. In the latter case, only the photons from the transition $(1s2s)_1 \rightarrow (1s^2)_0$ contribute the second-step synthetic spectra, but the photons emitted from the former step [i.e., $(1s2p_{3/2})_2 \rightarrow (1s2s)_1$] have no contribution to the spectra since their much lower energy is out of the energy range of the second-step spectra. Nevertheless, in the calculation of the alignment parameters of the state $(1s2s)_1$, the alignment transfer from this transition should be considered.

For the alignment transfer from the doubly excited states to the singly excited states, as well as from the transition mentioned above $(1s2p_{3/2})_2 \rightarrow (1s2s)_1$, two methods are used in the present calculations as discussed above. For the first method, the alignment parameters of the singly excited states are calculated by using the deorientation factor U_k [Eq. (4)] and are listed in Tables III and IV. For some of the transitions involved, only $\mathcal{A}^s_2$ is not enough to obtain the corresponding angular distribution coefficients W_{2nd}. For the singly excited states with total angular momentum $J \geqslant 2$, for instance, the corresponding intrinsic anisotropy parameter $\alpha^{sg}_4 \neq 0$ and thus $\mathcal{A}^s_4$ is also required for the calculation of the angular distribution coefficients W_{2nd}. The alignments $\mathcal{A}^s_4$ of the singly excited states obtained herein are listed in Table IV. One can see that only the alignment $\mathcal{A}^s_4$ of the singly excited state $(1s2p_{3/2})_2$ is nonzero, which is transferred from two doubly excited states $(2p_{1/2}2p_{3/2})_2$ and $(2p^2_{3/2})_2$ separately. Besides the method of the deorientation factor, the density matrix theory is also used to calculate the alignment parameters of the singly excited

TABLE III. Calculated alignment parameters for the doubly excited states $|d\rangle$ and the singly excited states $|s\rangle$. Here $\mathcal{A}^d_2$ is calculated with Eq. (3), $\mathcal{A}^s_2$ is calculated with the deorientation factor (5), and $\mathcal{A}^s_{2q}(q = -2 \text{ to } 2)$ is calculated with the density matrix theory (6). (The parameters $\mathcal{A}^s_{2\pm1}$ are all equal to zero and are not listed in the table for brevity.)

$\|d\rangle$		$\|s\rangle$		$\mathcal{A}^d_2$	$\mathcal{A}^s_2$	$\mathcal{A}^s_{2\pm2}$	$\mathcal{A}^s_{20}$
8	$(2s^2)_0$	6	$(1s2p_{3/2})_1$	0	0	0	0
12	$(2p^2_{1/2})_0$			0	0	0	0
14	$(2p_{1/2}2p_{3/2})_2$			−0.621	−0.367	−0.002	−0.001
16	$(2p^2_{3/2})_2$			−0.775	−0.459	0.001	−0.023
17	$(2p^2_{3/2})_0$			0	0	0	0
13	$(2p_{1/2}2p_{3/2})_1$	5	$(1s2p_{3/2})_2$	0.050	0.030	0	0.002
14	$(2p_{1/2}2p_{3/2})_2$			−0.621	−0.310	−0.011	−0.047
16	$(2p^2_{3/2})_2$			−0.775	−0.388	−0.016	−0.052
8	$(2s^2)_0$	3	$(1s2p_{1/2})_1$	0	0	0	0
12	$(2p^2_{1/2})_0$			0	0	0	0
13	$(2p_{1/2}2p_{3/2})_1$			0.050	−0.025	0.001	−0.001
14	$(2p_{1/2}2p_{3/2})_2$			−0.621	−0.367	−0.002	−0.001
16	$(2p^2_{3/2})_2$			−0.775	−0.459	0.001	−0.023
9	$(2s2p_{1/2})_0$	1	$(1s2s)_1$	0	0	0	0
10	$(2s2p_{1/2})_1$			0.183	−0.091	0.004	−0.004
11	$(2s2p_{3/2})_2$			−0.830	−0.491	0.003	−0.030
15	$(2s2p_{3/2})_1$			−1.407	0.704	−0.046	0.037

TABLE IV. Calculated alignment parameters for the doubly excited states $|d\rangle$ and the singly excited states $|s\rangle$. Here $\mathcal{A}^d_4$ is calculated with Eq. (3), $\mathcal{A}^s_4$ is calculated with the deorientation factor (5), and $\mathcal{A}^s_{4q}(q = -4 \text{ to } 4)$ is calculated with the density matrix theory (6). (The parameters $\mathcal{A}^s_{4\pm4}$, $\mathcal{A}^s_{4\pm3}$, and $\mathcal{A}^s_{4\pm1}$ are all equal to zero and are not listed in the table for brevity.)

$\|d\rangle$		$\|s\rangle$		$\mathcal{A}^d_4$	$\mathcal{A}^s_4$	$\mathcal{A}^s_{4\pm2}$	$\mathcal{A}^s_{40}$
8	$(2s^2)_0$	6	$(1s2p_{3/2})_1$	0	0	0	0
12	$(2p^2_{1/2})_0$			0	0	0	0
14	$(2p_{1/2}2p_{3/2})_2$			−0.966	0	−0.026	0.032
16	$(2p^2_{3/2})_2$			−0.275	0	−0.003	0.004
17	$(2p^2_{3/2})_0$			0	0	−0.003	0.004
13	$(2p_{1/2}2p_{3/2})_1$	5	$(1s2p_{3/2})_2$	0	0	0.001	−0.001
14	$(2p_{1/2}2p_{3/2})_2$			−0.966	0.644	−0.026	0.032
16	$(2p^2_{3/2})_2$			−0.275	0.183	−0.003	0.004
8	$(2s^2)_0$	3	$(1s2p_{1/2})_1$	0	0	0	0
12	$(2p^2_{1/2})_0$			0	0	0	0
13	$(2p_{1/2}2p_{3/2})_1$			0	0	0	0
14	$(2p_{1/2}2p_{3/2})_2$			−0.966	0	0.001	−0.001
16	$(2p^2_{3/2})_2$			−0.275	0	−0.026	0.032
9	$(2s2p_{1/2})_0$	1	$(1s2s)_1$	0	0	0	0
10	$(2s2p_{1/2})_1$			0	0	0	0
11	$(2s2p_{3/2})_2$			−0.031	0	0	0
15	$(2s2p_{3/2})_1$			0	0	−0.026	0.032

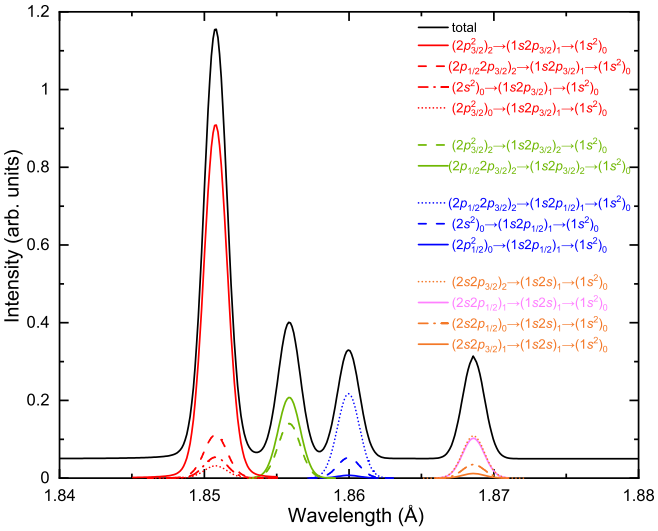

FIG. 3. Same as Fig. 2 but for the second-step decay photons.

states. In the calculations, all tensor components are required due to a breakage of the axial symmetry of the singly excited states. In Tables III and IV we list the alignments $\mathcal{A}^s_{2q}$ and $\mathcal{A}^s_{4q}$ of the singly excited states, respectively. As can be seen from the tables, the alignment parameters $\mathcal{A}^s_{2q}$ of the singly excited states with zero angular momentum are zero, which are the same as the results calculated with the deorientation factor. In contrast, it is different from the case of $\mathcal{A}^s_{4q}$. It should be noted that the alignment parameters $\mathcal{A}^d_2$ of the doubly excited states can affect the parameters $\mathcal{A}^s_{4q}$ and this is different from the case with the deorientation factor used, where $\mathcal{A}^s_4$ only depends on $\mathcal{A}^d_4$. Therefore, $\mathcal{A}^s_{4q}$ may be nonvanishing even if $\mathcal{A}^d_4$ is zero, which can be deduced from Eq. (6) and also can be seen from the results listed in Table IV.

In order to synthesize the second-step spectra as shown in Fig. 3, the resonance strengths, angular distribution coefficients, and polarizations corresponding to the second-step radiative decay are also calculated and are listed in Table V. From this table one can find that the angular distribution coefficients and polarizations calculated with the two methods mentioned above are different, especially for the polarizations. This difference intrinsically stems from the different treatments for these parameters by the two methods. For the method using the deorientation factor U_k [Eq. (4)], a relatively simple formula is emplyed to calculate the angular distribution coefficients and polarizations. For a particular transition, i.e., a particular intrinsic anisotropy parameter, the angular distribution coefficient and polarization depend only on the alignment parameters of the singly excited state. In contrast, in the framework of the density matrix theory, the two parameters are influenced also by the angular distribution coefficient $W_{1\mathrm{st}}$ of the first-step photon. Only the alignment parameter with the component $q_2 = 0$ (denoted by $\mathcal{A}^s_k$ to distinguish it from that obtained by using the density matrix theory) is taken into account in the first method and other components are neglected. However, due to a lack of axial symmetry of the decay system, all the components should be considered to describe the singly excited states. Therefore, it is more appropriate to use the density matrix theory to calculate the alignment transfer. Moreover, the two methods treat the alignment transfer in different ways. For the method using the deorientation factor, a simple proportional relationship is used to describe the alignment transfer from the doubly excited states to the singly excited ones. However, in the density matrix theory, Eq. (6) shows that the alignment transfer depends on both

TABLE V. Similar to Table I but for the second-step radiative decay from the singly excited states $|s\rangle$ to the ground state $|g\rangle$. Here $W(U)$ and $P(U)$ are the angular distribution coefficient and the degree of linear polarization calculated with the deorientation factor, respectively; W and P have similar meanings but are calculated within the framework of the density matrix theory.

$\lvert d\rangle$		$\lvert s\rangle$		$\lvert g\rangle$	$\hbar\nu'$	B	$W(U)$	W	$P(U)$	P	$S_{2\mathrm{nd}}$	K_c
8	$(2s^2)_0$	6	$(1s2p_{3/2})_1$	$(1s^2)_0$	6699.0	1	1	1	0	0	1.174	0.807
12	$(2p^2_{1/2})_0$					1	1	1	0	0	0.003	0.807
14	$(2p_{1/2}2p_{3/2})_2$					1	1.130	1.128	0.345	0.038	2.406	0.816
16	$(2p^2_{3/2})_2$					1	1.162	1.173	0.419	0.285	18.344	0.874
17	$(2p^2_{3/2})_0$					1	1	1	0	0	0.688	0.807
13	$(2p_{1/2}2p_{3/2})_1$	5	$(1s2p_{3/2})_2$	$(1s2s)_1\rightarrow(1s^2)_0$	45.5	0.176	0.994	0.998	−0.019	−0.016	0.002	0.809
				$(1s^2)_0$	6680.6	0.824	1.009	1	0.026	0	0.009	0.809
14	$(2p_{1/2}2p_{3/2})_2$			$(1s2s)_1\rightarrow(1s^2)_0$		0.176	1.065	0.874	0.183	0.437	0.947	0.819
				$(1s^2)_0$		0.824	0.649	0.835	0.234	−0.087	4.233	0.788
16	$(2p^2_{3/2})_2$			$(1s2s)_1\rightarrow(1s^2)_0$		0.176	1.081	0.840	0.225	0.513	0.750	0.877
				$(1s^2)_0$		0.824	0.811	0.831	−0.278	−0.671	3.468	0.650
8	$(2s^2)_0$	3	$(1s2p_{1/2})_1$	$(1s^2)_0$	6665.9	1	1	1	0	0	1.045	0.809
12	$(2p^2_{1/2})_0$					1	1	1	0	0	0.141	0.809
13	$(2p_{1/2}2p_{3/2})_1$					1	1.009	1.010	0.026	0	0.006	0.809
14	$(2p_{1/2}2p_{3/2})_2$					1	1.130	1.128	0.345	0.038	4.283	0.819
16	$(2p^2_{3/2})_2$					1	1.162	1.173	0.419	0.285	0.027	0.877
9	$(2s2p_{1/2})_0$	1	$(1s2s)_1$	$(1s^2)_0$	6635.1	1	1	1	0	0	0.679	0.811
10	$(2s2p_{1/2})_1$					1	1.032	1.037	−0.094	0	1.997	0.811
11	$(2s2p_{3/2})_2$					1	1.174	1.189	−0.444	−0.368	2.380	0.722
15	$(2s2p_{3/2})_1$					1	0.751	0.712	0.993	0	0.229	0.811

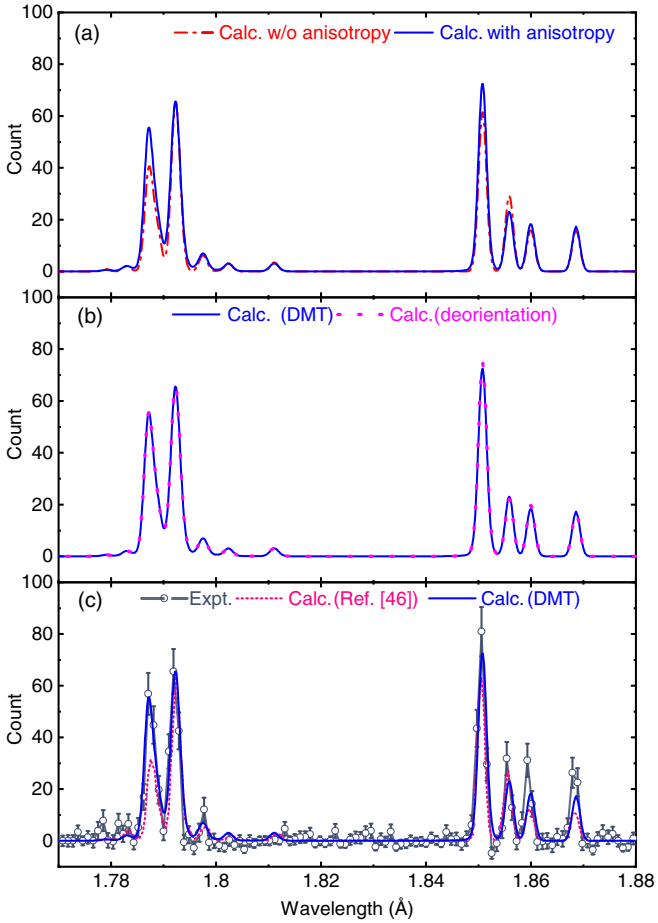

FIG. 4. (a) Comparison of the synthetic spectra using the density matrix theory with (blue solid line) and without (red dashed line) taking anisotropy and correction of crystal diffraction into account. (b) Comparison of the synthetic spectra using two methods, i.e., the deorientation factor (magenta dotted line) and density matrix theory (blue solid line). (c) Comparison of the synthetic spectrum using density matrix theory with the calculation (pink dotted line) and experimental results (gray solid line with open circles) in Ref. [46].

the observation angles and the angular distribution coefficients $W_{1\mathrm{st}}$ of the first-step photons. In fact, if one takes an integration over the observation angles, Eq. (6) could be simplified to Eq. (5) [39,50]. Furthermore, when neglecting the angular distribution coefficients $W_{1\mathrm{st}}$ of the first-step photon and other $q \neq 0$ components of $\mathcal{A}^s_{kq}$, Eqs. (13), (16), and (17) in the density matrix theory can be reduced to Eqs. (11), (14), and (15), respectively, for the method using the deorientation factor. The above discussion suggests that the two methods are consistent, but the method using the density matrix theory is more complete, especially for a case where the symmetry is broken.

By further comparing the angular distribution coefficients calculated by using the two different methods, it can be found that the difference is very small except for the singly excited state $(1s2p_{3/2})_2$, which is mainly due to a different treatment of its alignment parameters with $k_2 = 4$, while other singly excited states are affected by only the alignment parameters with $k_2 = 2$ but not those with $k_2 = 4$ as their angular momenta are less than 2. Moreover, the polarizations obtained with the two different methods show a distinct deviation. Nevertheless, since the polarization correction to the crystal diffraction efficiency is small, such a distinct deviation will not cause a significant difference in the spectra obtained with the two methods.

C. Synthetic spectra

By using the method described in Sec. III C, the overall synthetic spectra can be obtained, which are plotted in Fig. 4. Figure 4(a) presents a comparison of the synthetic spectra obtained herein using the density matrix theory with (blue solid line) and without (red dashed line) taking the anisotropy and correction of crystal diffraction into account. For the case using the formalism of the deorientation factor, the results are similar and are not shown in the figure for clarity. In Fig. 4(b) we show the comparison of the synthetic spectra obtained by the two methods mentioned above. One can find that there is no significant difference between the two theoretical spectra for the system of DR of hydrogenlike Fe^{25+} ions. Figure 4(c) displays the final synthetic spectra (including the anisotropy and correction of crystal diffraction) together with that calculated by Nakamura *et al* [46] as well as the experimental results [46] for comparison. As can be seen clearly, the present theoretical simulation reproduces very well the experimental results. It is also found that the present results with the anisotropy and polarization correction included agree much better with the experimental results than the results without the correction [46]. For the first-step decay photons, the main peaks are perfectly matched. In contrast, a slight discrepancy is obtained for the second-step photons. This can be explained partially by the poor statistics of the experiment and maybe also by the fact that the interference between the two-step photons [36] is not included in the present calculations.

V. CONCLUSION

The *KLL* DR of hydrogenlike Fe^{25+} ions has been studied by using the FAC package based on the relativistic configuration-interaction method. In order to synthesize the DR spectra and compare with the existing experimental results, the anisotropy and polarization of x-ray line emissions were also investigated by considering an alignment transfer from the doubly excited states to the singly excited states. The alignment transfer was treated with two different methods, that is, the formalism of the deorientation factor and the density matrix theory. It was found that the present DR synthetic spectra reproduce very well the existing experimental results. A slight discrepancy obtained between theory and experiment could be due to the poor statistics of the experiment and the interference between the two-step decay photons [36]. More precise experiments are strongly required, in particular, for the *K*-shell satellite lines of highly charged Fe ions, which are a concern of the astrophysical community. The data presented in this work should be helpful in the analysis and interpretation of next-generation astronomical observations [55] in which microcalorimeters with higher-energy resolution will be used.

ACKNOWLEDGMENTS

The authors acknowledge Professor Nobuyuki Nakamura for providing the original experimental data. This work was supported by the National Natural Science Foundation of China (Grants No. 12074352, No. 11675158, and No. 11804280), the CAEP Foundation (Grant No. CX2019022), and the Fundamental Research Funds for the Central Universities in China (Grants No. YJ202143 and No. YJ202144).

[1] N. Trueba, J. M. Miller, A. C. Fabian, J. Kaastra, T. Kallman, A. Lohfink, D. Proga, J. Raymond, C. Reynolds, M. Reynolds, and A. Zoghbi, Astrophys. J. Lett. **899**, L16 (2020).

[2] A. Corral, M. J. Page, F. J. Carrera, X. Barcons, and M. G. Watson, Astron. Astrophys. **492**, 71 (2008).

[3] M. M. Tatum, T. J. Turner, S. A. Sim, L. Miller, J. N. Reeves, A. R. Patrick, and K. S. Long, Astrophys. J. **752**, 94 (2012).

[4] F. Tombesi, M. Cappi, J. N. Reeves, G. G. C. Palumbo, T. Yaqoob, V. Braito, and M. Dadina, Astron. Astrophys. **521**, A57 (2010).

[5] L. Č. Popović, E. G. Mediavilla, P. Jovanović, and J. A. Muñoz, Astron. Astrophys. **398**, 975 (2003).

[6] N. V. Voshchinnikov, T. Henning, M. S. Prokopjeva, and H. K. Das, Astron. Astrophys. **541**, A52 (2012).

[7] J. Deprince, M. A. Bautista, S. Fritzsche, J. A. Garcia, T. Kallman, C. Mendoza, P. Palmeri, and P. Quinet, Astron. Astrophys. **626**, A83 (2019).

[8] J. Deprince, M. A. Bautista, S. Fritzsche, J. A. Garcia, T. R. Kallman, C. Mendoza, P. Palmeri, and P. Quinet, Astron. Astrophys. **635**, A70 (2020).

[9] N. L. S. Jeffrey, P. Saint-Hilaire, and E. P. Kontar, Astron. Astrophys. **642**, A79 (2020).

[10] S. V. Vadawale, T. Chattopadhyay, N. P. S. Mithun, A. R. Rao, D. Bhattacharya, A. Vibhute, V. B. Bhalerao, G. C. Dewangan, R. Misra, B. Paul, A. Basu, B. C. Joshi, S. Sreekumar, E. Samuel, P. Priya, P. Vinod, and S. Seetha, Nat. Astron. **2**, 50 (2018).

[11] Q. Abarr, H. Awaki, M. G. Baring, R. Bose, G. De Geronimo, P. Dowkontt, M. Errando, V. Guarino, K. Hattori, K. Hayashida, F. Imazato, M. Ishida, N. K. Iyer, F. Kislat, M. Kiss, T. Kitaguchi, H. Krawczynski, L. Lisalda, H. Matake, Y. Maeda, *et al.*, Astropart. Phys. **126**, 102529 (2021).

[12] R. Taverna, W. Zhang, M. Dovčiak, S. Bianchi, M. Bursa, V. Karas, and G. Matt, Mon. Not. R. Astron. Soc. **493**, 4960 (2020).

[13] K. Akiyama, J. C. Algaba, A. Alberdi, W. Alef, R. Anantua, K. Asada, R. Azulay, A.-K. Baczko, D. Ball, M. BalokoviÄ, J. Barrett, B. A. Benson, D. Bintley, L. Blackburn, R. Blundell, W. Boland, K. L. Bouman, G. C. Bower, H. Boyce, M. Bremer, *et al.*, Astrophys. J. Lett. **910**, L12 (2021).

[14] H. Feng, H. Li, X. Long, R. Bellazzini, E. Costa, Q. Wu, J. Huang, W. Jiang, M. Minuti, W. Wang, R. Xu, D. Yang, L. Baldini, S. Citraro, H. Nasimi, P. Soffitta, F. Muleri, A. Jung, J. Yu, G. Jin, *et al.*, Nat. Astron. **4**, 511 (2020).

[15] M. C. Weisskopf, E. H. Silver, H. L. Kestenbaum, K. S. Long, and R. Novick, Astrophys. J. **220**, L117 (1978).

[16] M. Chauvin, H. G. Florén, M. Friis, M. Jackson, T. Kamae, J. Kataoka, T. Kawano, M. Kiss, V. Mikhalev, T. Mizuno, N. Ohashi, T. Stana, H. Tajima, H. Takahashi, N. Uchida, and M. Pearce, Sci. Rep. **7**, 7816 (2017).

[17] B. Zhang, Nature (London) **587**, 45 (2020).

[18] Dipti, S. W. Buechele, A. C. Gall, S. Sanders, C. I. Szabo, R. Silwal, E. Takacs, and Y. Ralchenko, J. Phys. B **53**, 115701 (2020).

[19] C. Shah, N. Hell, A. Hubbard, M. F. Gu, M. J. MacDonald, M. E. Eckart, R. L. Kelley, C. A. Kilbourne, M. A. Leutenegger, F. S. Porter, and G. V. Brown, Astrophys. J. **914**, 34 (2021).

[20] A. C. Gall, Dipti, S. W. Buechele, S. Sanders, C. I. Szabo, R. Silwal, Y. Ralchenko, N. Brickhouse, and E. Takacs, J. Phys. B **53**, 145004 (2020).

[21] P. Beiersdorfer, N. Hell, and J. K. Lepson, Astrophys. J. **864**, 24 (2018).

[22] P. Beiersdorfer, J. Phys. B **48**, 144017 (2015).

[23] S. P. Preval, N. R. Badnell, and M. G. O'Mullane, Phys. Rev. A **93**, 042703 (2016).

[24] Z. Hu, J. Yang, G. Xiong, J. Zhang, and B. Zhang, in Proceedings of Japan-China-Korea Joint Seminar on Atomic and Molecular Processes in Plasma, Chengdu, 2016, edited by D. Kato, Z. Cui, and C. Dong, National Institute for Fusion Science Report No. NIFS-PROC-103 (unpublished), p. 111.

[25] S. Fritzsche, A. Surzhykov, and T. Stöhlker, Phys. Rev. Lett. **103**, 113001 (2009).

[26] Z. Hu, X. Han, Y. Li, D. Kato, X. Tong, and N. Nakamura, Phys. Rev. Lett. **108**, 073002 (2012).

[27] Z. Hu, Y. Li, X. Han, D. Kato, X. Tong, H. Watanabe, and N. Nakamura, Phys. Rev. A **90**, 062702 (2014).

[28] H. Jörg, Z. Hu, H. Bekker, M. A. Blessenohl, D. Hollain, S. Fritzsche, A. Surzhykov, J. R. Crespo López-Urrutia, and S. Tashenov, Phys. Rev. A **91**, 042705 (2015).

[29] C. Shah, H. Jörg, S. Bernitt, S. Dobrodey, R. Steinbrügge, C. Beilmann, P. Amaro, Z. Hu, S. Weber, S. Fritzsche, A. Surzhykov, J. R. Crespo López-Urrutia, and S. Tashenov, Phys. Rev. A **92**, 042702 (2015).

[30] P. Amaro, C. Shah, R. Steinbrügge, C. Beilmann, S. Bernitt, J. R. Crespo López-Urrutia, and S. Tashenov, Phys. Rev. A **95**, 022712 (2017).

[31] X.-M. Tong, Z. Hu, Y. Li, X. Han, D. Kato, H. Watanabe, and N. Nakamura, J. Phys. B **48**, 144002 (2015).

[32] Y. Li, P. Li, B. Duan, Z. Wu, and J. Yan, J. Phys. B **48**, 174001 (2015).

[33] N. Nakamura, J. Phys. B **49**, 212001 (2016).

[34] C. Shah, P. Amaro, R. Steinbrügge, C. Beilmann, S. Bernitt, S. Fritzsche, A. Surzhykov, J. R. Crespo López-Urrutia, and S. Tashenov, Phys. Rev. E **93**, 061201(R) (2016).

[35] C. Shah, P. Amaro, R. Steinbrügge, S. Bernitt, J. R. Crespo López-Urrutia, and S. Tashenov, Astrophys. J. Suppl. Ser. **234**, 27 (2018).

[36] S. Zakowicz, W. Scheid, and N. Grün, J. Phys. B **37**, 131 (2004).

[37] A. Surzhykov, U. D. Jentschura, T. Stöhlker, and S. Fritzsche, Phys. Rev. A **73**, 032716 (2006).

[38] S. Fritzsche, N. M. Kabachnik, and A. Surzhykov, Phys. Rev. A **78**, 032703 (2008).

[39] O. Matula, S. Fritzsche, F. J. Currell, and A. Surzhykov, Phys. Rev. A **84**, 052723 (2011).
[40] K. Blum, *Density Matrix Theory and Applications*, Springer Series on Atomic, Optical, and Plasma Physics Vol. 64 (Springer, Berlin, 2012).
[41] D. R. DeWitt, D. Schneider, M. W. Clark, M. H. Chen, and D. Church, Phys. Rev. A **44**, 7185 (1991).
[42] H. Watanabe, A. P. Kavanagh, H. Kuramoto, Y. M. Li, N. Nakamura, S. Ohtani, B. E. O'Rourke, A. Sato, H. Tawara, X. M. Tong, and F. J. Currell, Nucl. Instrum. Methods Phys. Res. Sect. B **235**, 261 (2005).
[43] B. E. O'Rourke, F. J. Currell, H. Kuramoto, S. Ohtani, H. Watanabe, Y. M. Li, T. Tawara, and X. M. Tong, Phys. Rev. A **77**, 062709 (2008).
[44] Z. Hu, Y. Li, and N. Nakamura, Phys. Rev. A **87**, 052706 (2013).
[45] D. Bernhardt, C. Brandau, Z. Harman, C. Kozhuharov, A. Muller, W. Scheid, S. Schippers, E. W. Schmidt, D. Yu, A. N. Artemyev, I. I. Tupitsyn, S. Bohm, F. Bosch, F. J. Currell, B. Franzke, A. Gumberidze, J. Jacobi, P. H. Mokler, F. Nolden, U. Spillman, *et al.*, Phys. Rev. A **83**, 020701(R) (2011).
[46] N. Nakamura, H. Tobiyama, H. Nohara, A. P. Kavanagh, H. Watanabe, H. A. Sakaue, Y. Li, D. Kato, F. J. Currell, C. Yamada, and S. Ohtani, J. Phys.: Conf. Ser. **58**, 267 (2007).
[47] M. F. Gu, Can. J. Phys. **86**, 675 (2008).
[48] P. Beiersdorfer, D. A. Vogel, K. J. Reed, V. V. Decaux, J. H. Scofield, K. Widmann, G. Holzer, E. Forster, O. Wehrhan, D. W. Savin, and L. Schweikhard, Phys. Rev. A **53**, 3974 (1996).
[49] Z. Hu, Experimental studies on dielectronic recombination of highly charged heavy ions, Ph.D. thesis, University of Electro-Communications, 2012.
[50] V. V. Balashov, A. Grum-Grzhimailo, and N. Kabachnik *Polarization and Correlation Phenomena in Atomic Collisions: A Practical Theory Course*, 1st ed., Physics of Atoms and Molecules (Springer, New York, 2000).
[51] K. N. Lyashchenko and O. Y. Andreev, Phys. Rev. A **91**, 012511 (2015).
[52] M. S. del Rio and R. J. Dejus, in *Advances in Computational Methods for X-Ray and Neutron Optics*, Proceedings of the SPIE 49th Annual Meeting on Optical Science and Technology, Denver, 2004, edited by M. S. del Rio (SPIE, Bellingham, 2004), pp. 171–174.
[53] G. W. F. Drake, Phys. Rev. A **34**, 2871 (1986).
[54] D. Banaś, A. Gumberidze, S. Trotsenko, A. V. Volotka, A. Surzhykov, H. F. Beyer, F. Bosch, A. Bräuning-Demian, S. Fritzsche, S. Hagmann, C. Kozhuharov, A. Kumar, X. Ma, R. Mann, P. H. Mokler, D. Sierpowski, U. Spillmann, S. Tashenov, Z. Stachura, A. Warczak, and T. Stöhlker, Phys. Rev. A **87**, 062510 (2013).
[55] N. Hell, P. Beiersdorfer, G. V. Brown, M. E. Eckart, R. L. Kelley, C. A. Kilbourne, M. A. Leutenegger, T. E. Lockard, F. S. Porter, and J. Wilms, X-Ray Spectrom. **49**, 218 (2020).